Article:
Pering, T.D., Tamburello, G., McGonigle, A.J.S. et al. (4 more authors) (2014) High time resolution fluctuations in volcanic carbon dioxide degassing from Mount Etna. Journal of Volcanology and Geothermal Research, 270. 115 - 121. ISSN 0377-0273

https://doi.org/10.1016/j.jvolgeores.2013.11.014

High time resolution fluctuations in volcanic carbon dioxide degassing from Mount Etna - DOI: 10.1016/j.jvolgeores.2013.11.014

Pering T.D.[a]*, Tamburello G.[b], McGonigle A.J.S.[a,c], Aiuppa A.[b,c], Cannata A.[d], Giudice G.[c], Patanè D.[d]

* Corresponding author, ggp12tdp@sheffield.ac.uk, Department of Geography, Winter Street University of Sheffield, Sheffield, S10 2TN, United Kingdom, +447838219369

[a]University of Sheffield, Dept. of Geography, Winter Street, S10 2TN, United Kingdom

[b]DiSTeM, Università di Palermo, via Archirafi, 22, 90123 Palermo, Italy

[c]Istituto Nazionale di Geofisica e Vulcanologia, Sezione di Palermo, Via Ugo La Malfa, 153, 90146, Palermo, Italy

[d]Istituto Nazionale di Geofisica e Vulcanologia, Osservatorio Etneo, Piazza Roma, 2, 95125 Catania, Italy

Abstract - We report here on the first record of carbon dioxide gas emission rates from a volcano, captured at ≈ 1 Hz. These data were acquired with a novel technique, based on the integration of UV camera observations (to measure SO_2 emission rates) and field portable gas analyser readings of plume CO_2/SO_2 ratios. Our measurements were performed at the North East crater of Mount Etna, southern Italy, and the data reveal strong variability in CO_2 emissions over timescales of tens to hundreds of seconds, spanning two orders of magnitude. This carries important implications for attempts to constrain global volcanic CO_2 release to the atmosphere, and will lead to an increased insight into short term CO_2 degassing trends. A common oscillation in CO_2 and SO_2 emission rates in addition to the CO_2/SO_2 ratios was observed at periods of ≈ 89 s. Our results are furthermore suggestive of an intriguing temporal lag between oscillations in CO_2 emissions and seismicity at periods of ≈ 300 – 400 s, with peaks and troughs in the former series leading those in the latter by ≈ 150 s. This work

opens the way to the acquisition of further datasets with this methodology across a range of basaltic systems to better our understanding of deep magmatic processes and of degassing links to manifest geophysical signals.

Carbon Dioxide; Passive Degassing; Volcanic remote sensing; Plume imaging; Volcano seismology;

1. Introduction

Carbon dioxide (CO_2) is among the most abundant constituents of volcanic gases (Carroll and Holloway, 1994), and exsolves from magmas deeper than other common volatiles such as sulphur dioxide (SO_2) and water vapour (H_2O) (Giggenbach, 1996). Knowledge of CO_2 emissions can therefore contribute significantly to our understanding of the movement of magmas in deep volcanic plumbing systems. Hitherto, the measurement of CO_2 emission rates has been challenging due to the difficulty of resolving volcanogenic CO_2 above high background atmospheric levels. In consequence, attempts to routinely measure plume CO_2 emission rates, particularly at high time resolution, have been rather limited (Aiuppa et al., 2006; 2010). Therefore, notwithstanding the significant contributions made in constraining CO_2 emission rates of volcanic plumes at targets such as Mt. Erebus, Antarctica (Wardell et al., 2004), Ol Doinyo Lengai, Tanzania (Koepenick et al., 1996), White Island, New Zealand (Werner et al., 2008), Ruapehu, New Zealand (Werner et al., 2006), Redoubt, Alaska (Werner et al., 2012a; 2012b), Stromboli, Italy (Aiuppa et al., 2010; 2011), Mt. Etna, Italy (Allard, 1991) and Kilauea, USA (Poland et al., 2012), these data remain relatively spartan, and in general lack information regarding temporal changes. This remains a fundamental weakness in attempts to constrain global volcanogenic CO_2 emission rate budgets, in view of which there is a pressing demand for the development and application of novel

methodologies to improve constraints on spatio-temporal volcanic CO_2 degassing and our comprehension of volcanic systems.

Recently, the Multi-GAS technique (Shinohara, 2005; Aiuppa et al., 2005) has been pioneered to enable rapid measurements of volcanic plume chemical compositions, including CO_2/SO_2 gas ratios, leading to significant advances in our understanding of degassing processes. Furthermore, in the last years, UV camera imagery has been applied in volcanology, enabling acquisition of SO_2 emission rates with time resolutions of ≈ 1 Hz, many orders of magnitude faster than possible in the past (e.g., Mori and Burton, 2006; Tamburello et al., 2011a). Here we report on the first volcanic deployment of a novel technique, by which volcanic CO_2 emission rates are captured with an acquisition frequency of ≈ 1 Hz, based on the integration of the above two approaches. Such a capability will increases the future potential of linking degassing to geophysical data on unprecedented timescales with significant applicability in improving hazard analysis (Gerlach et al., 2002) and eruption forecasting measures (Aiuppa et al., 2007; Poland et al., 2012).

The CO_2 emission rate data were captured during a field campaign on Mt. Etna (37.734°N, 15.004°E), an alkaline strato-volcano whose CO_2-rich magmas (Spilliaert et al., 2006) result in the volcano being the largest time averaged contributor to global volcanic emissions of CO_2 (Allard et al., 1991; Gerlach 1991). Etna currently has four degassing summit areas: the South-East crater (SEC), the Central Craters (Bocca Nuova and Voragine), and the North-East crater (NEC) (Fig. 1). Our study is based on passive emissions from the NEC, in recent times one of the most actively degassing vents on Etna (Aiuppa et al., 2008) and the site of recurrent eruptive activity in the last few decades (Allard et al., 2006).

2. Methodology

The SO_2 emission rates were captured using two Apogee Alta U260 cameras, fitted with 16 bit 512 x 512 pixel Kodak KAF-0261E thermo-electrically cooled CCD array detectors. A Pentax B2528-UV lens of f = 25 mm was attached to the front of each camera, providing ≈ 24° field of view. The lenses were fitted with filters of 10 nm FWHM (Asahi Bunko Inc.), one centred around 310 nm, where plume SO_2 absorbs incident UV radiation, and the other at 330 nm, where no such absorption occurs. Qualitative plume absorbances captured in the camera plume images were converted to column amounts via a calibration procedure involving four quartz cells containing known SO_2 column amounts: 100, 200, 1000, 2000 ppm m; SO_2 values within the plume were always within this range. The calibrations were performed at the time of measurement, by viewing clear sky adjacent to the plume, resulting in R^2 values > 0.99 for the linear fitting. As the measurement conditions were favourable: e.g., the plume was transparent, the background sky was cloudless and the plume was < 4 km distant, additional DOAS based calibrations were not performed, as there is an excellent match between DOAS and cell based calibrations under such conditions (Lübcke et al., 2013). Under such circumstances we speculate that the measurement error was low, however, as radiative transfer has yet to become a routinely considered element of UV camera retrievals it is hard to provide an exact error budget in this case (e.g., Kern et al., 2009). For full details on all data capture, retrieval and calibration procedures please see Kantzas et al., (2010). All of these protocols were executed using the Vulcamera code (Tamburello et al., 2011b).

The UV camera was located at the Pizzi Deneri observatory which provided a clear vantage point of the NEC plume, at a distance of ≈ 2 km (Fig. 1); the data were acquired between 08:45 and 09:45 GMT on the 12th of September 2012. Integrated column amount (ICA)

values were determined by summing SO_2 concentrations over the plume profile, perpendicular to its transport vector (Fig. 1). The emission rates (kg s^{-1}) were then found by multiplying ICAs by the plume transport speed, with the latter arising from cross-correlation analysis of the propagation of the plume across the field of view over a sequence of camera images (e.g. see McGonigle et al., 2005; Williams-Jones et al., 2006). The plume speed varied very little over the acquisition period (≈ 13.4 m s^{-1} throughout). The camera capture rate ranged between 0.5-1 Hz depending upon incident light levels, hence linear interpolation was applied, where necessary, to produce a uniform 1 Hz SO_2 emission rates dataset.

The CO_2/SO_2 degassing ratios of the NEC were measured with a field portable Multi-GAS unit (Shinohara, 2005; Aiuppa et al., 2005) located ≈ 100 m downwind of the crater's vent, at a site chosen to avoid signal contamination from low-temperature fumarolic discharges (Shinohara et al., 2008). This unit extractively sampled the plume gases, providing CO_2 and SO_2 concentration readings at ≈ 0.5 Hz measurement frequency. The SO_2 concentrations were measured with an electrochemical sensor (City Technology, sensor type 3ST/F), of calibration range 0-200 ppm, and manufacturer quoted accuracy of ± 2%, repeatability of 1% and a resolution of 0.5 ppmv. The CO_2 concentrations were measured with an infrared sensor (Edinburgh Instruments, Gascard II), of 0-3000 ppmv range, and with an accuracy ±2 % and a resolution of 0.8 ppmv. Prior to the campaign, the Multi-GAS sensors were calibrated in the laboratory using standard gas cylinders of concentrations within the sensor ranges (e.g., 10 and 100 ppm SO_2 and 3,000 ppm CO_2; all in nitrogen matrixes) and gas mixtures corresponding approximately to plume conditions (e.g., 10-30 ppm SO_2 in air; e.g., with 380-900 ppm CO_2). Pure nitrogen was used as zero reference in each case. These laboratory characterisations confirmed a typical measurement error in the CO_2/SO_2 ratios of ≤ 15%.

An additional calibration test was performed to measure the response characteristics of the Multi-GAS sensors to rapid changes in gas fumigation, under the range of conditions we encountered during our field study. This was achieved by connecting three gas bottles of the following compositions: 79% N_2, 21% O_2 (e.g., the eluent); 79% N_2, 21% O_2, 3010 ppm CO_2; 79% N_2, 21% O_2, 100 ppm SO_2, via regulators to the Multi-GAS inlet, to provide an overall flow rate of 1.2 l min^{-1} into the instrument (e.g., as is typically the case for Multi-GAS field sampling). Firstly, the typical plume conditions were mimicked by setting the eluent flux to 0.72 l min^{-1}, and the CO_2 and SO_2 bottle fluxes to 0.24 l min^{-1} each, which led to gas concentrations at the sensor of 615 ppm and 20.4 ppm, respectively, for CO_2 and SO_2. The registered Multi-GAS ratios for such conditions are shown in Fig. 2 for $t < 70$ s and $t>130$ s, leading to corresponding ratio errors of < 5%. We also simulated rapid increases and decreases in gas concentration at the sensor ($t \approx 80$ s, 125 s; Fig. 2) to correspond to those we observed in the field, both in terms of timescale and magnitude, corresponding to the arrival and departure of more intense volcanogenic gas parcels. This was achieved by switching the eluent flux to/from 0.5 l min^{-1} and the CO_2 and SO_2 fluxes concurrently to/from 0.35 l min^{-1}, altering the concentrations to/from 29 ppm and 878 ppm, respectively for SO_2 and CO_2. As shown in Fig. 2, the ratio in error remained within ±15% during these transitions, confirming the ability of the Multi-GAS to respond rapidly to these changes in plume fumigation, given typical $t_{90\%}$ values of ≈ 10 s for both the Multi-GAS SO_2 and CO_2 sensors ($t_{90\%}$ corresponds to the time between standard gas injection and the instrumental signal reaching 90% of the plateau value). Hence, this provides confidence that any field observed changes in gas ratios could not be artefacts of differing instrumental response times. Indeed, Fig 3b shows a zoomed section of the acquired Multi-GAS time-series showing the similar response characteristics of the two sensors to volcanogenic changes in the concentrations of both species. Atmospheric background CO_2 values were determined by plotting raw CO_2 values

148 with SO_2 on a scatter plot. The intercept of the regression line with the axis is taken as the
149 background level, in this case a value of ≈ 200 ppm. Temporal synchronicity with the UV
150 camera SO_2 emission rate data series, throughout the one hour observation period, was
151 ensured by time referencing both instruments' data series with GPS receiver outputs. Linear
152 interpolation was applied to the Multi-GAS ratio data to temporally match these data to the 1
153 Hz UV camera SO_2 emission rates.
154
155 The ICA determination for the NEC SO_2 emission rate calculation was made ≈ 180 m
156 downwind of the GPS receiver geo-referenced multi-GAS measurement location. The UV
157 camera derived plume speeds were then used to derive temporal lags between the gas
158 emission rate and gas ratio time series (≈ 13 s throughout the acquisition), enabling shifting
159 of the series relative to one another by this lag value to account for the slight offset between
160 the plume locations viewed/sampled by the two techniques. This procedure provided
161 excellent overlap between peaks and troughs in the gas concentration and emission rate series
162 as the volcanogenic source signal fluctuated (Fig. 3b) and also serves to offset the small
163 Multi-GAS sensor lag. A lag of ≈ 13 s is also achieved when cross-correlating the UV camera
164 SO_2 emission rate with Multi-GAS SO_2 readings, further corroborating our procedure.
165

166 **3. Results and Discussion**

167 The acquired NEC Multi-GAS CO_2 vs. SO_2 concentrations are plotted in Fig. 3a,
168 demonstrating a general trend (with a mean molar ratio of 0.5±0.07, based on the largest, e.g.,
169 ±15%, uncertainty encountered during our laboratory sensor characterisations) between
170 emissions of the two species, with the exception of large spikes in CO_2 emissions within the
171 shaded grey oval. Since the Multi-GAS measurement location was chosen with great care to
172 completely avoid fumarolic discharges, we exclude the possibility that this feature could arise

173 from contamination by these sources. Given that these spikes were also closely temporally
174 aligned to peaks in seismicity, the source of which was located under the NEC at the time of
175 measurements, as discussed further below, this is also suggestive that these trends were
176 indeed related to activity at the NEC.
177
178 Each molar CO_2/SO_2 gas ratio datum (Fig. 3d), was converted to a mass ratio on the basis of
179 the species' relative molecular weights and then multiplied by the temporally coincident SO_2
180 emission rate (Fig. 3f) to deliver the CO_2 emission rate time series shown in Fig. 3e,
181 demonstrating significant variability in emissions, spanning two orders of magnitude (from ≈
182 0.1 to 12 kg s^{-1}), over timescales of tens to hundreds of seconds. These fluxes are subject to
183 errors of ±15% arising from the gas ratios, on the basis of our aforementioned experimental
184 characterisations, however errors arising from the SO_2 fluxes are not considered here for the
185 reasons detailed above. This observation of fluctuation in CO_2 degassing, in tandem with our
186 reported methodology, has the potential to add to our understanding of CO_2 degassing trends
187 and of their importance in volcanic loading of the atmosphere.
188
189 The acquisition averaged NEC CO_2/SO_2 molar ratio of 0.5±0.07 was low although not
190 unusual for this crater, where the degassing activity is often sourced by more evolved (e.g.,
191 more volatile-depleted) magmas than those supplying the central craters' (CCs) plumes
192 (Aiuppa et al., 2006; 2008). Likewise, the mean NEC CO_2 emission rate and SO_2 emission
193 rates captured in our dataset were also rather low, although not unprecedentedly so: at 2 kg s^{-1}
194 and 6 kg s^{-1}, respectively. On the day of the measurements the majority of Etna's degassing
195 arose from the CCs, with combined Voragine and Bocca Nuova CO_2 and SO_2 emission rates
196 of 86 kg s^{-1} and 14 kg s^{-1}, respectively; these data were acquired by us with our Multi-GAS
197 and UV camera unit and are consistent with previous evaluations (e.g., Aiuppa et al., 2008).

198 Whilst this NEC contribution was only a fraction of Etna's gas budget, these observations do
199 provide the opportunity, for the first time, to characterise the short term CO_2 degassing
200 behaviour of an active volcano, and any periodicities observed therein. Studying this
201 behaviour for the other craters will be a key target of future work.
202
203 Periodicity in SO_2 release, on short timescales, has been reported from a few volcanoes
204 worldwide (e.g., Boichu et al., 2010; Nadeau et al., 2011; Tamburello et al., 2012, 2013).
205 Periodicity was investigated in our CO_2, SO_2 and contemporaneous geophysical data using a
206 continuous Morlet wavelet transform technique (see Fig. 4). This approach involves scaling a
207 defined oscillation (a Morlet wavelet), and mathematically assessing similarities between the
208 acquired data and the scaled wavelet. This signal processing technique is often used in the
209 analysis of environmental processes due to its effectiveness in detecting natural oscillations
210 (Morlet et al., 1982), such as climatic variability (Jevrejeva et al., 2003). This technique is
211 preferred to other time series analysis as information is gleaned on the stability of
212 periodicities present at a given time. Given the duration of our acquisition, the longest
213 resolvable oscillation period via this analysis was 512 s according to the Nyquist theorem
214 (Nyquist, 2002), hence the plots in Fig. 4 are cropped accordingly.
215
216 Fig. 4 shows non-stationary degassing behaviour in the NEC CO_2 and SO_2 Morlets with
217 characteristic periodicities between ≈ 40-500 s. Oscillations in this period range are also
218 apparent in Morlet analysis of contemporaneously acquired seismic data (Fig. 4d). The
219 dominant modulation frequencies in the degassing data were assessed with power spectral
220 densities (PSDs) using Welch's method (Welch, 1967), applied after normalization of the
221 data. The resultant periodograms show the power of manifest oscillations across this period
222 range (see Fig. 4), revealing the dominant peak for CO_2 emission rates at ≈ 89 s; a peak

matching this period is also evident in the SO_2 data, and the dominant peak in CO_2/SO_2 ratios also falls here (≈ 85 s). The latter result strongly implies that the observed non-stationary degassing signals are indeed volcanogenic in origin and not an artefact of atmospheric transport processes which would not generate any modulation in sampled gas ratios. Furthermore, the presence of the ≈ 89 s signal in both CO_2 and SO_2 emission rate PSDs suggests that a common source process is generating the periodicity in both cases.

There are many physical processes which could potentially drive the observed modulations in gas emission rates and ratios. These include: (1) convection of magma in the conduit and/or the shallow to deep plumbing system (Kazahaya et al., 1994; Boichu et al., 2010); as convection is likely a non-stationary process, this could involve varying overturn rate, leading to modulation in gas release; (2) pulsatory supply of volatile rich magmas into the conduit; on Mt. Erebus, this has been proposed to introduce a consequent periodicity in emissions at the magma surface (Oppenheimer et al., 2009); (3) changes in the volatile content of the magma or supply of volatiles from depth (Kazahaya et al., 2002), in which depressurisation based exsolution of gases from the melt could, itself, lead to a periodicity in gas sourcing; (4) short to long term changes in rheology of the magma (Koyaguchi et al., 1993); such trends in magma viscosity would act to vary gas transit speed throughout the plumbing system; and (5) interaction of magma and entrained volatiles with geometric discontinuities in the conduit or shallow storage zones (James et al., 2006; Palma et al., 2011); such features could cause periodic collection and release of bubbles, by analogy with the collapsing foam model for strombolian activity (Jaupart and Vergniolle, 1988; Vergniolle and Brandeis, 1994). Further work based on an expanded dataset is now required to investigate, in more detail, the relevance of each of these models in this volcanic context, by assessing the variation and stability of emission rate periodicities in time and their links to geophysical signals.

In the context of this study we investigated the relationship between periodicities manifested in the various captured datasets. This was achieved by correlating the coefficients produced by the Morlet wavelet analysis for the CO_2 and SO_2 emission rate and seismic data (Fig. 5), in order to establish the degree to which oscillations at a particular period demonstrated common strength and phase between the series. This is preferable to correlating the raw signals as it eliminates rapid variability, hence more clearly resolves where dominant fluctuations are shared across the data streams. There is a clear link between the periodicities present in CO_2 and SO_2 emissions up to ≈ 250 s where the link breaks down for around 50 s, before resuming, then peaking at ≈ 500 s (Fig. 5a). Note that discussion of a possible gas-infrasonic relationship is not included here as any link, if present, was obscured by high wind pollution in the acoustic dataset. The seismic vs. CO_2 emission rate analysis reveals an intriguing negative correlation (< -0.5; Fig. 5b) for periods between 300 and 400 s, which corresponds to the period range where the relationship between CO_2 and SO_2 emissions breaks down (Fig. 5a).

This anti-correlation is suggestive of a possible temporal lag between oscillations at these frequencies in the seismic and CO_2 emission rate series, which we investigated further by performing, each second, a mathematical integration of the Morlet coefficients, between 300 and 400 s for the seismic, CO_2/SO_2 and CO_2 emission rate series, to generate the output shown in Fig. 6b. These three traces all show distinctive peaks between ≈ 08:50 and ≈ 09:00 GMT, e.g., the time intervals shaded grey in Figs. 3 and 6, where elevated wavelet coefficients in this period range (Figs. 4a, b and d) demonstrated strong oscillations therein, and the CO_2/SO_2 ratios spikes to high values (Fig. 3a). The two gas peaks in the shaded area of Fig. 6b preceded those in the seismic record by 100-150 s, and indeed, moving forward the

seismic record in time by 125 s and correlating led to a correlation coefficient of ≈ 0.9 in this time window. Therefore, given the absence of any seismic events prior to these gas spikes, this could well imply the existence of a process causing elevated CO_2 emissions to be released from the vent some 150 s prior to peaks in seismicity. Transit time of gas from the source to measurement location is < 30 s. Our observations might also be indicative of a model of quite the opposite nature, in that a small NW displacement in tremor location occurred at a depth of ≈ 500-1000 m between ≈ 09:10 - 09:15 (Personal Communication, Giuseppe Di Grazia, INGV), is followed by several large peaks in gas emissions, ≈ 500-900 s later, which corresponds to realistic travel times for gas rise from such depths (Manga, 1996).

Regardless of the possible lag direction, a mechanism involving the movement of magma and/or entrained volatiles, induced by changes in pressure or temperature, could be invoked. Peaks in the gases' CO_2/SO_2 ratios could be caused by a deeper than average pressure base i.e. a greater source depth. A system-wide increase in temperature could also drive a long-term increase in ratios by facilitating the transport of volatiles from depth; a localised temperature increase, through injection of fresh magma, might also therefore, in theory, temporarily reproduce the same effect. Each of these processes could generate seismicity, due to migration of magmas and/or volatiles, followed by elevated gas emissions. An opposite hypothesis could involve a model based on readjustment of the magma level, with corresponding seismic energy generation, following release of gases at the surface. These tentative hypotheses, based on our initial observations, are presented as avenues for future work, in which longer datasets are required to further investigate the direction of any manifest lag between seismic and degassing data, with a view to better characterising the associated underground magmatic processes.

4. Concluding Remarks

Here we report for the first time the combined use of a field portable Multi-GAS sensor and UV camera imaging to produce a high time resolution (≈ 1 Hz) volcanic CO_2 emission rate dataset, in this case from Mt. Etna's North East crater. The development of such a methodology has significant implications for the study of short and long term degassing trends and improved integration between degassing and geophysical datasets. We demonstrate that CO_2 emissions are highly variable, spanning two orders of magnitude, on timescales of tens to hundreds of seconds. This technique is therefore significant in respect of attempts to assess global volcanogenic CO_2 emission rates. We furthermore establish that both the CO_2 emission rates and SO_2 emission rates, in addition to the CO_2/SO_2 ratios, exhibit prominent common periodicities at ≈ 89 s and that our results are suggestive of an intriguing lag between CO_2 and seismic oscillations, with periods of around 300 – 400 s, possibly indicative of a process involving the movement of magma in the conduit. This work paves the way for further high time resolution investigations into degassing of CO_2 at Mount Etna and other basaltic volcanoes worldwide to expand our understanding of degassing dynamics and links to manifest geophysical signals.

Acknowledgements

TDP and AMcG acknowledge the support of a NERC studentship, the University of Sheffield and a Google Faculty Research award. AA acknowledges support from the European Research Council Starting Independent Research Grant (agreement number 1305377). Data presented in this paper were obtained during the "Etna – Pizzi Deneri field trip" organized and supported by the Università degli Studi di Palermo and INGV sezione di Catania and Palermo. We thank Giuseppe Di Grazia (INGV sezione di Catania) for seismic tremor

321 locations. We are finally grateful to Cynthia Werner and Toshiya Mori for their reviews
322 which have greatly improved the quality of this paper.

323 **References**

324 Aiuppa, A., Federico, C., Paonita, A., Giudice, G., Valenza, M., 2005. Chemical mapping of
325 a fumarolic field: La Fossa Crater, Vulcano Island (Aeolian Islands, italy). Geophys. Res.
326 Lett. 13 (L13309), doi:10.1029/2005GL023207

327 Aiuppa, A., Federico, C., Giudice, G., Gurrieri, S., Liuzzo, M., Shinohara, H., Favara, R.,
328 Valenza, M., 2006. Rates of carbon dioxide plume degassing from Mount Etna volcano. J.
329 Geophs. Res. 111 (B09207), doi:10.1029/2006JB004307

330 Aiuppa, A., Moretti, R., Federico, C., Giudice, G., Gurrieri, S., Liuzzo, M., Papale, P.,
331 Shinohara, H., Valenza, M., 2007. Forecasting Etna eruption by real time evaluation of
332 volcanic gas composition. Geology 35 (12), 1115-1118

333 Aiuppa, A., Giudice, G., Gurrieri, S., Liuzzo, M., Burton, M., Caltabiano, T., McGonigle, A.
334 J. S., Salerno, G., Shinohara, H., Valenza, M., 2008. Total volatile flux from Mount Etna,
335 Geophys. Res. Lett. 35 (L24302), doi:10.1029/2008GL035871

336 Aiuppa, A., Burton, M., Caltabiano, T., Giudice, G., Guerrieri, S., Liuzzo, M., Mure, F.,
337 Salerno, G., 2010. Unusually large magmatic CO_2 gas emissions prior to a basaltic paroxysm,
338 Geophys. Res. Lett. 37 (L17303), doi:10.1029/2010GL043837

339 Aiuppa, A., Burton, M., Allard, P., Caltabiano, T., Giudice, G., Gurrieri, S., Liuzzo, M.,
340 Salerno, G., 2011. First observational evidence for the CO2-driven origin of Stromboli's
341 major explosions. J. Geophs. Res-Sol. Ea. 2 (2), 135-142, doi :10.5194/se-2-135-2011

342 Allard, P., Carbonnelle, J., Dajlevic, D., Le Bronec, J., Morel, P., Robe, M. C., Maurenas, J.
343 M., Faivre-Pierret, R., Martin, D., Sabroux, J.C., Zettwoog, P., 1991. Eruptive and diffuse
344 emissions of CO_2 from Mount Etna. Nature 351, 387-391

345 Allard, P., Behncke, B., D'Amico, S., Neri, M., Gambino, S., 2006. Mount Etna 1993-2005:
346 Anatomy of an evolving eruptive cycle. Earth-Sci. Rev. 78, 85-114

347 Boichu, M., Oppenheimer, C., Tsanev, V., Kyle, P., 2010. High temporal resolution SO_2 flux
348 measurements at Erebus volcano, Antarctica. J. Volcanol. Geotherm. Res. 190, 325-336

349 Caltabiano, T., Burton, M., Giammanco, S., Allard, P., Bruno, N., Murè, F., Romano, R.,
350 2004. Volcanic gas emissions from the summit craters and flanks of Mt. Etna, 1987– 2000.
351 In: Bonaccorso, A., Calvari, S., Coletelli, M., Del Negro, C., Falsaperla, S. (Eds.), Mt. Etna:
352 Volcano Laboratory. AGU, Washington, D. C., pp. 111-128

353 Carroll, M. R., Holloway, J. R., (Eds.) 1994. Volatiles in Magmas. Mineralogical Society of
354 America Reviews in Mineralogy 30, Washington, D. C.

355 Gerlach, T. M., 1991. Present-day CO_2 emissions from volcanoes. EOS Trans. AGU 72
356 (249), 254-255

357 Gerlach, T. M., McGee, K. A., Elias, T., Sutton, A. J., Doukas, P., 2002. Carbon dioxide
358 emission rate of Kilauea Volcano: Implications for primary magma and the summit reservoir.
359 J. Geophys. Res. 107 (B9), 2189, doi:10.1029/2001JB000407

360 Giggenbach, W. F., 1996. Chemical composition of volcanic gases. In: Scarpa, R., Tilling, R.
361 I. (Eds.), Monitoring and Mitigation of Volcanic Hazards. Springer, New York, pp. 221-256

James, M. R., Lane, S. J., Chouet, B. A., 2006. Gas slug ascent through changes in conduit diameter: Laboratory insights into a volcano-seismic source process in low-viscosity magmas. J. Geophys. Res. 111 (B05201), doi:10.1029/2005JB003718

Jaupart, C., Vergniolle, S., 1988. Laboratory models of Hawaiian and Strombolian eruptions. Nature 331, 58-60

Jevrejeva, S., Moore, J. C., Grinsted, A., 2003. Influence of the Arctic Oscillation and El Niño-Southern Oscillation (ENSO) on ice conditions in the Baltic Sea: The wavelet approach. J. Geophys. Res. Atm. 108 (D21), doi:10.1029/2003JD003417

Kantzas, E.P., McGonigle, A. J. S., Tamburello, G., Aiuppa, A., Bryant, R. G., 2010. Protocols for UV camera volcanic SO_2 measurements. J. Volcano. Geotherm. Res. 194, 55-60

Kazahaya, K., Shinohara, H., Saito, G., 1994. Excessive degassing of Izu-Oshima volcano: magma convection in a conduit. B. Volcanol. 56, 207-216

Kazahaya, K, Shinohara, H., Saito, G., 2002. Degassing process of Satsuma-Iwojima volcano, Japan: Supply of volatile components from a deep magma chamber. Earth Planets Space 54, 327-335

Kern, C., Deutschmann, T., Vogel, L., Wöhrbach, M., Wagner, T., Platt, U. 2009. Radiative transfer corrections for accurate spectroscopic measurements of volcanic gas emissions. B. Volcanol. 72, 233-247, doi: 10.1007/s00445-009-0313-7

Koepenick, K. Brantley, S., Thompson, J., Rowe, G., Nyblade, A., Moshy, C., 1996. Volatile emissions from the crater and flank of Oldoinyo Lengai volcano, Tanzania. J. Geophys. Res. 10, 13,819-13,830

383 Koyaguchi, T., Hallworth, M. A., Huppert, H. E., 1993. An experimental study on the effects
384 of phenocrysts on convection in magmas. J. Volcan, Geotherm. Res. 55, 15-32

385 Lübcke, P., Bobrowski, N., Illing, S., Kern, C., Alvarez Nievez, J. M. Vogel, L., Zielcke, J.,
386 Delgado Granados H., Platt, U., 2013. On the absolute calibration of SO_2 cameras. Atmos.
387 Meas. Tech. 6, 677-696, doi:10.5194/amt-6-677-2013

388 Manga, M., 1996. Waves of bubbles in basaltic magmas and lavas. J. Geophys. Res. 101
389 (B8), 17,457-17,465

390 McGonigle, A. J. S., Hilton, D. R., Fischer, T. P., Oppenheimer, C., 2005. Plume velocity
391 determination for volcanic SO_2 flux measurements. Geophys. Res. Lett. 32 (L11302),
392 doi:10.1029/2005GL022470

393 Mori, T., Burton, M., 2006. The SO_2 camera: a simple, fast and cheap method for ground-
394 based imaging of SO2 in volcanic plumes. Geophys. Res. Lett. 33 (L24804),
395 doi:10.1209/2006GL027916

396 Morlet, J., Arens, G., Fougeau, E., Giard, D., 1982. Wave propagation and sampling theory;
397 Part I, Complex signal and scattering in multilayered media. Geophysics 47 (2), 203-221

398 Nadeau, P.A., Palma, J. L., Waite, G. P., 2011. Linking volcanic tremor, degassing, and
399 eruption dynamics via SO_2 imaging. Geophys. Res. Lett. 38 (L01304),
400 doi:10.1029/2010GL045820

401 Oppenheimer, C., Lomakina, A. S., Kyle, P. R., Kingsbury, N. G., Boichu, M., 2009.
402 Pulsatory magma supply to a phonolite lava lake. Earth Planet. Sci. Lett., 284, 392-398

403 Nyquist, H., 2002. Certain topics in telegraph transmission theory (Reprinted from
404 Transactions of the A. I. E. E., February, pg 617-644, 1928). Proceedings I. E. E. E. 90 (2),
405 280-305, doi:10.1109/5.989875

406 Palma, J. L., Blake, S., Calder, E. S., 2011. Constraints on the rates of degassing and
407 convection in basaltic open-vent volcanoes. Geochem. Geophy. Geosy. 12 (11),
408 doi :10.1029/2011GC003715

409 Poland, M. P., Miklius, A., Sutton, A. J., Thornber, C. R., 2012. A mantle-driven surge in
410 magma supply to Kilauea Volcano during 2003-2007. Nat. Geosci. 5 (4), 295-297,
411 doi:10.1038/NGEO1426

412 Shinohara, H., 2005. A new technique to estimate volcanic gas composition: Plume
413 measurements with a portable multi-sensor system. J. Volcanol. Geotherm. Res. 143, 319–
414 333.

415 Shinohara, H., Aiuppa, A., Giudice, G., Gurrieri, S., Liuzzo, M., 2008. Variation of H_2O/CO_2
416 and CO_2/SO_2 ratios of volcanic gases discharged by continuous degassing of Mount Etna
417 volcano, Italy. J. Geophys. Res 113 (B09203), doi:10.1029/2007JB005185

418 Spilliaert, N., Allard, P., Métrich, N., Sobolev, A. V., 2006. Melt inclusion record of the
419 conditions of ascent, degassing, and extrusion of volatile-rich alkali basalt during the
420 powerful 2002 flank eruption of Mount Etna (Italy). J. Geophys. Res. 111 (B04203),
421 doi:10.1029/2005JB003934

422 Tamburello, G., Kantzas, E. P., McGonigle, A. J. S., Aiuppa, A., 2011a. Recent advances in
423 ground-based ultraviolet remote sensing of volcanic SO_2 fluxes. Ann. Geophys. 54 (2), 199-
424 208

425 Tamburello, G., Kantzas, E. P., McGonigle, A. J. S., Aiuppa, A., 2011b. Vulcamera: a
426 program for measuring volcanic SO_2 using UV cameras. Ann. Geophys. 54 (2), 219-221

427 Tamburello, G., Aiuppa, A., Kantzas, E.P., McGonigle, A. J. S., Ripepe, M., 2012. Passive
428 vs. active degassing modes at an open-vent volcano (Stromboli, Italy). Earth and Planetary
429 Science Letters 359-360, 106-116

430 Tamburello, G., Aiuppa, A., McGonigle, A. J. S., Allard, P., Cannata, A., Giudice, G.,
431 Kantzas, E.P., Pering, T. D., 2013. Periodic volcanic degassing behaviour: The Mount Etna
432 example. Geophys. Res. Lett. 40 (1-5), doi:10.1002/grl.50924

433 Vergniolle, S., Brandeis, G., 1994. Origin of the sound generated by Strombolian explosions.
434 J. Geophys. Res. 21, 1959-1962

435 Wardell, L. J., Kyle, P.R., Chaffin, C., 2004. Carbon dioxide and carbon monoxide emission
436 rates from an alkaline intra-plate volcano: Mt. Erebus, Antarctica. J. Volcan. Geotherm. Res.
437 131 (1-2), 109-121

438 Welch, P.D., 1967. The Use of Fast Fourier Transform for the Estimation of Power Spectra:
439 A Method Based on Time Averaging Over Short, Modified Periodograms. IEEE Transactions
440 on Audio Electroacoustics AU-15 (2), 70–73

441 Werner, C., Christenson, B.W., Hagerty, M., Britten, K., 2006. Variability of volcanic gas
442 emissions during a crater lake heating cycle at Ruapehu Volcano, New Zealand. J. Volcan.
443 Geotherm. Res. 154 (3-4), 291-302

444 Werner, C., Hurst, T., Scott, B., Sherburn, S., Christenson, B. W., Britten, K., Cole-Baker, J.,
445 Mullan, B., 2008. Variability of passive gas emissions, seismicity, and deformation during
446 crater lake growth at White Island Volcano, New Zealand, 2002-2006. J. Geophs. Res-Sol.
447 Ea. 113 (B1), doi:10.1029/2007JB005094

Werner, C., Evans, W. C., Kelly, P. J., McGimsey, R., Pfeffer, M., Doukas, M., Neal, C., 2012a. Deep magmatic degassing versus scrubbing: Elevated CO_2 emissions and C/S in the lead-up to the 2009 eruption of Redoubt Volcano, Alaska. Geochem. Geophy. Geosy. 13 (3), doi:10.1029/2011GC003794

Werner, C., Kelly, P. J., Doukas, M., Lopez, T., Pfeffer, M., McGimsey, R., Neal, C., 2012b. Degassing of CO_2, SO_2, and H_2S associated with the 2009 eruption of Redoubt Volcano, Alaska. J. Volcanol. Geotherm. Res. doi:10.1016/j.volgeores.2012.04.012

Williams-Jones, G., Horton, K. A., Elias, T., Garbeil, H., Mouginis-Mark, P. J., Sutton, A. J., Harris, A. J. L., 2006. Accurately measuring volcanic plume velocity with multiple UV spectrometers. B. Volcanol. 68, 328-332, doi:10.1007/s00445-005-0013-x

460 **Figures and Captions**

461 Fig. 1: Map of the summit of Mount Etna showing the craters (NE – North East Crater,
462 Voragine, Bocca Nuova, SE – South East Crater), EBCN seismic station, the Multi-GAS
463 location and (a) the plume direction; the left inset shows the volcano location in Sicily; the
464 right inset shows the NE crater plume on the acquisition day as viewed with the UV camera
465 from Pizzi Deneri, with the colour scale indicating ppm m column amounts of SO_2 over the
466 image pixels; (b) shows the plume cross-section used to determine the Integrated Column
467 Amount (ICA) within this inset; and (c), within the main image, the viewing vector
468 corresponding to this profile with respect to the Multi-GAS location.

469 Fig. 2: Multi-GAS laboratory measurements characterising the passing of a cloud of elevated
470 concentration CO_2 (black line) and SO_2 (grey line) gases, simulating the plume "puffs" we
471 measured on Etna. The Multi-GAS derived CO_2/SO_2 molar ratio (blue line) and ratio error
472 (red line) demonstrate rapid instrumental responses to these transient changes with minimal
473 associated uncertainty (< 15%).

474 Fig. 3: a) Background air corrected CO_2 versus SO_2 concentrations, from the Multi-GAS
475 instrument observations; the mean molar gas ratio (0.5) is determined as the gradient of the
476 best fit regression line; the grey-filled area indicates a peak in CO_2; b) UV SO_2, Multi-GAS
477 CO_2 and SO_2 readings showing excellent overlap between peaks and troughs and
478 demonstrating equal temporal response characteristics to changes in the volcanogenic signal
479 from the two Multi-GAS sensors; c) Multi-GAS CO_2 and SO_2 time series captured over the
480 acquisition period; d) the molar ratio of CO_2/SO_2; e) the CO_2 emission rate and f) SO_2
481 emission rate across the acquisition period.

482 Figure 4: Morlet wavelets (normalised) for a) CO_2/SO_2 ratio; b) CO_2 emission rate; c) SO_2
483 emission rate and d) seismicity during the acquisition period showing periodicities in the

484 range 40-500 s; Welch power spectral density plots are also shown, indicating the dominant
485 frequencies in each case.

486 Fig. 5: Correlation matrices produced by calculating linear correlation between coefficients
487 extracted from the Morlet wavelets in SO_2 emission rate, CO_2 emission rate and seismicity, at
488 steps of 1 s. Strong correlation is evident between CO_2 and SO_2 emission in a); whilst
489 negative correlation for periods between 300 and 400 s is apparent in b); see main text for
490 further details.

491 Fig. 6: a) the RMS vertical component of seismicity from the EBCN station, in the 0.5-5.5 Hz
492 range; b) the wavelet components (integrated over the 300-400s period range) of the CO_2/SO_2
493 ratio, CO_2 emission rate and seismic RMS are compared, showing, between ≈ 08:50 and
494 09:00 GMT (the grey shaded area), a lag of ≈ 100-150 s between peaks and troughs in CO_2
495 emissions and seismicity.

496

497

498

499

500

501

502

503

504

505 **Figure 1**

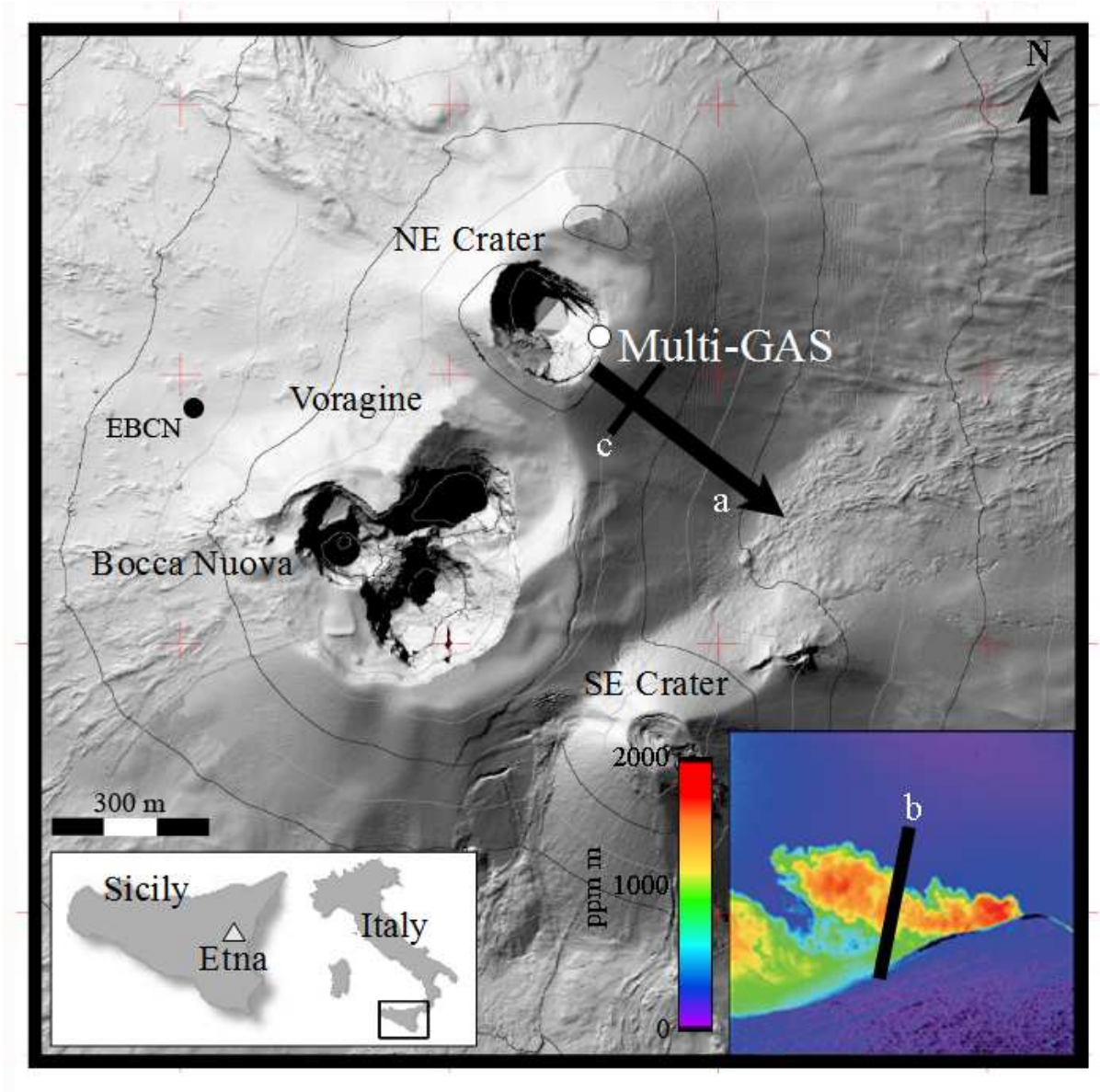

506

507

508

509

510

511

512 **Figure 2**

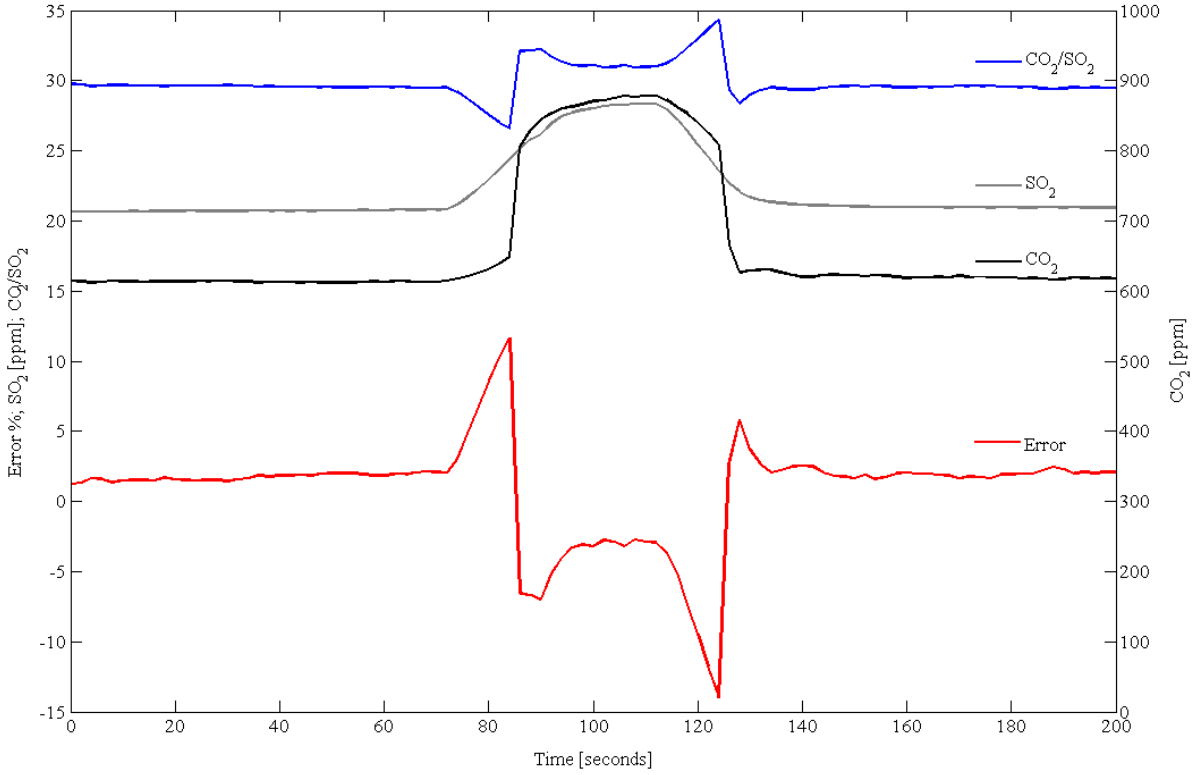

513

514

515

516

517

518

519

520

521

522

Figure 3

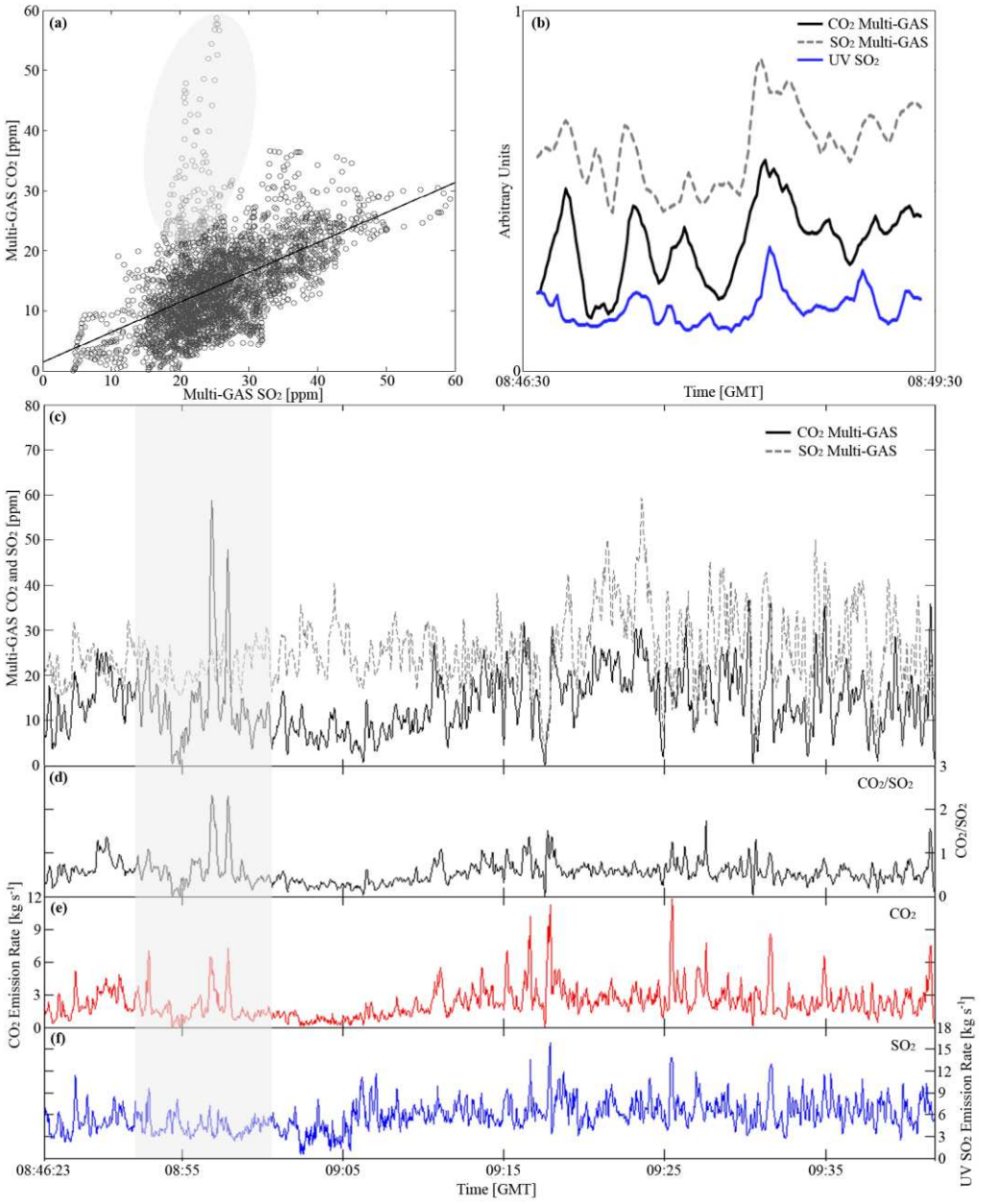
(a)
Multi-GAS CO2 [ppm]
Multi-GAS SO2 [ppm]
(b)
CO2 Multi-GAS
SO2 Multi-GAS
UV SO2
Arbitrary Units
08:46:30
08:49:30
Time [GMT]
(c)
CO2 Multi-GAS
SO2 Multi-GAS
Multi-GAS CO2 and SO2 [ppm]
(d)
CO2/SO2
CO2/SO2
(e)
CO2
CO2 Emission Rate [kg s-1]
(f)
SO2
UV SO2 Emission Rate [kg s-1]
08:46:23
08:55
09:05
09:15
09:25
09:35
Time [GMT]

529 **Figure 4**

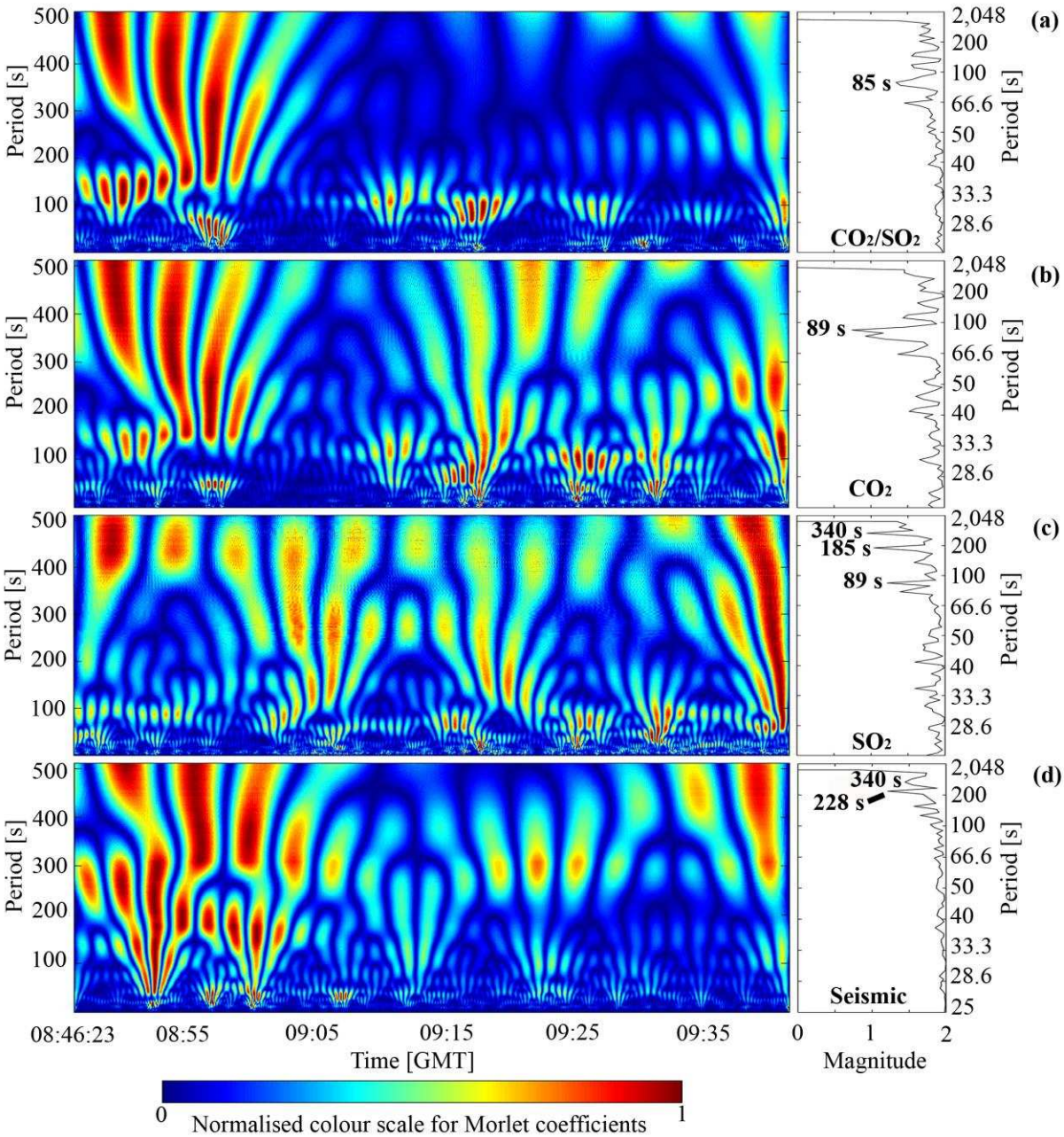

530

531

532

533

534

Figure 5

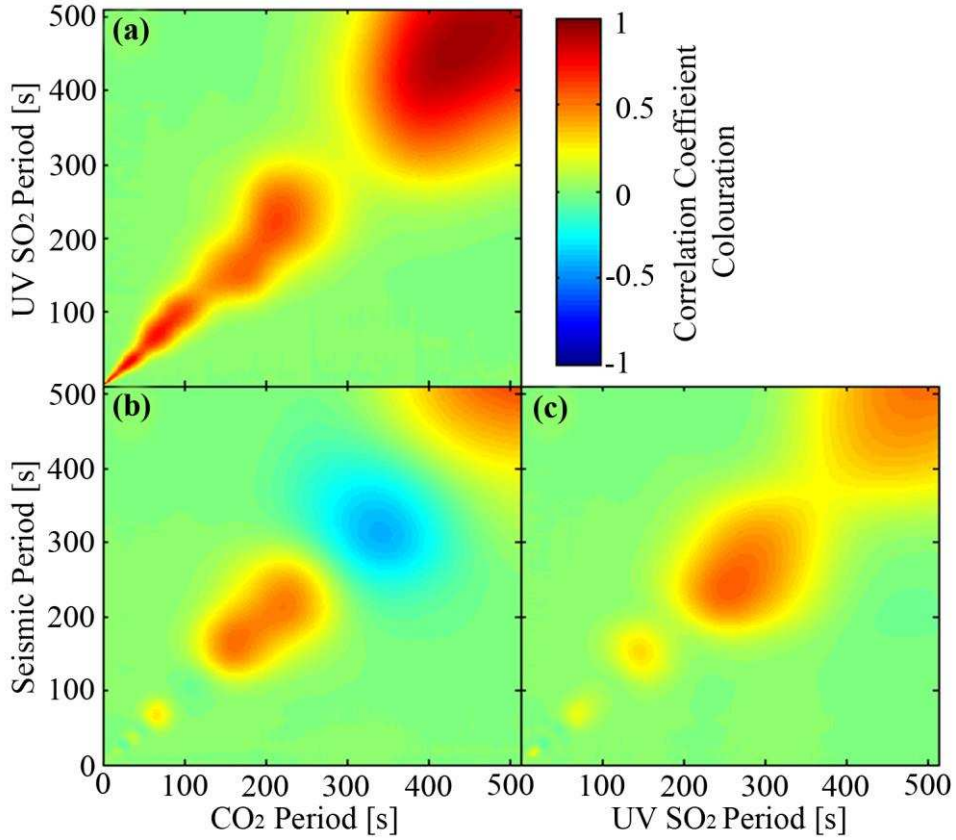

546 **Figure 6**

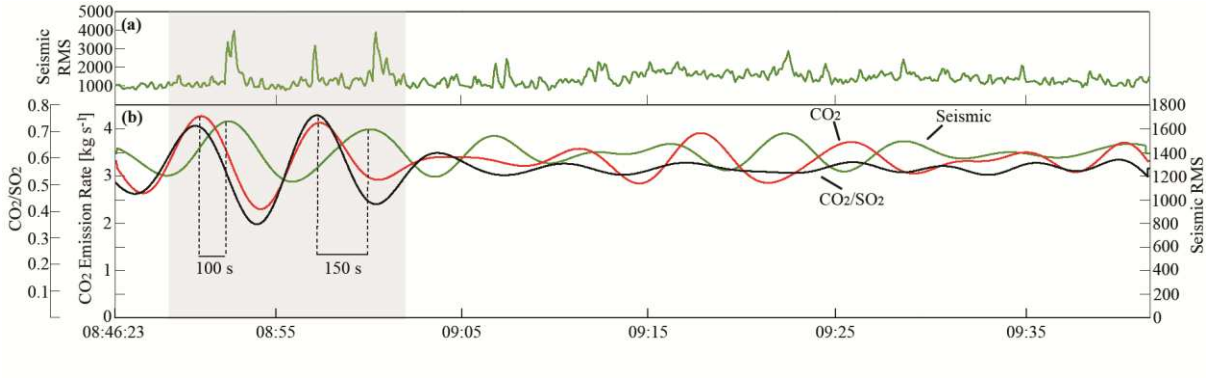

547